Lanczos-Based Model-Order Reduction for Optimization and Control of Electromagnetically Induced Hyperthermia

Marc E. Kowalski and Jian-Ming Jin
Department of Electrical and Computer Engineering
University of Illinois at Urbana-Champaign
Urbana, Illinois 61801

Abstract—**In this work, two procedures for the optimization of transient temperature fields in electromagnetically induced therapeutic hyperthermia are proposed. Both procedures employ numerical models of electromagnetic and heat transfer processes. The computational demands of the optimization procedures are mitigated by employing reduced-order numerical models obtained via the spectral Lanczos decomposition method (SLDM) in lieu of the original, high-order models. An open-loop optimization procedure based on quadratic programming (QP) is proposed that determines the time dependent RF power level necessary to reach therapeutic temperatures quickly without exposing healthy tissue to excessive temperatures. Additionally, a closed-loop optimization procedure is proposed based on linear-quadratic Gaussian (LQG) optimal control that employs feedback from temperature measurements such as those available from magnetic resonance thermography. The performance of both techniques is simulated on a realistic tissue model of the human trunk heated by an annular phased array (APA). It is shown that by optimizing the transient temperature fields in oncological hyperthermia, effective thermal dose can be increased for a fixed treatment time and level of risk to healthy tissue. Additionally, it is shown that in some cases the non-linear nature of the human thermoregulatory response (manifest as temperature dependent perfusion) can be compensated for by the proposed linear feedback controller.**

Index Terms: *Keywords*— **reduced-order models, hyperthermia, linear-quadratic control, bio-heat transfer.**

I. Introduction

Recent clinical successes [1] have continued to drive the development of electromagnetic hyperthermia technology for oncological applications. Primarily used in addition to radiation therapy, hyperthermia, or the elevation of cancerous tissue temperatures, has been shown to have clinical value in a number of studies despite serious technical difficulties [2]. It has long been recognized that computational simulations can aid both in development of better applicator designs [3] and in patient-specific optimization of treatments [4].

One of the greatest technical challenges for non-invasive hyperthermia is the heating of "deep-seated" tumors (those residing more than 7 cm below the surface of the skin). The annular phased-array (APA) [5] has proven to be a promising applicator for this type of heating. A typical APA applicator consists of a set of independent radiators placed in a circumferential array around the patient, with a bolus filled with chilled water placed between the radiators and patient to provide impedance matching and superficial cooling. The individual phases and amplitudes of each array element may then be adjusted, allowing interference effects to be exploited to selectively heat the tumor. A significant amount of research has been conducted in the optimization of the specific absorption rate (SAR) [4], [6]–[8] as well as steady-state temperatures [6], [9], [10] for electromagnetic phased-array applicators. The potentially overwhelming computational demands of these optimization procedures has lead to research into ways to increase their efficiency for both ultrasound [11] and electromagnetic [12] heating systems.

Many previous studies of hyperthermia optimization [4], [6]–[12] employed time-invariant criteria (SAR or steady-state temperature) to define the notion of an optimal treatment. However, it is well known that the entire time-history of the tumor is required to establish a strong correlation between measurable quantities and treatment outcome [13]. It is therefore desirable for the clinician to be able to prescribe the time-histories of the temperature in the cancerous tissue [2], or at least be able to investigate the feasibility of doing this for a specific patient-applicator configuration. Indeed, early efforts in model-based optimization procedures for hyperthermia recognized the desirability of a *transient* temperature optimization capability [14]–[16]. These works, however, employed simplified one- and two-dimensional models of the hyperthermia process which are known to have severe limitations [17]. The absence of a report of the use of detailed, three-dimensional models of hyperthermia in transient optimization procedures reflects the potential computational difficulties associated with the use of numerical models of high-dimensionality in optimization procedures.

One way of avoiding the difficulties associated with high-order numerical models is to seek a low-order model which preserves important behaviors of the high-order model, a process known widely as model-order reduction (MOR). The use of MOR for hyperthermia has been

This material is based upon work supported under a National Science Foundation Graduate Fellowship and National Science Foundation Grant NSF ECE 94-57735.

proposed before in the context of feedback controller design [18], temperature and perfusion estimation [19], and applicator optimization [11]. A comparative study of reduced-order modeling approaches has been performed recently [20] which has resulted in a proposed extension to the balanced realization technique [21]. However, these works [11], [18]–[21] also employed one- and two-dimensional models of the hyperthermia process, which cannot, in general, capture all of the relevant physics [17]. The balanced realization technique used in these works is not suitable for use with the high-dimensional numerical models resulting from a full three-dimensional discretization. This is a consequence of the need for information from the entire observability and controllability gramians in order to compute a full-order coordinate transformation into balanced coordinates [22]. In fact, the highest-order thermal model of hyperthermia reported to have been reduced has an order of 450 [11], [20]. The construction of three-dimensional numerical models of oncological hyperthermia at spatial resolutions as coarse as 1 cm^3 quickly requires model orders several orders-of-magnitude greater than this.

In this work, a method is presented for model-order reduction that is suitable for reduction of high-order models resulting from full three-dimensional models of hyperthermia. The method is based on the spectral Lanczos decomposition method (SLDM) [23], [24], a variant of which has been applied successfully in the past to heat transfer modeling [25]. The SLDM, when used in conjunction with finite-difference or finite-element models of heat transfer, requires only inexpensive sparse matrix-vector products to construct a low-order partial tridiagonalization of the system which serves as the reduced-order model (ROM). The intention of this paper is to explore the suitability of the SLDM in the type of applications MOR has found in the past for hyperthermia. To achieve this, the SLDM is applied to open-loop optimization, closed-loop control, and closed-loop estimation of temperatures induced by electromagnetic applicators.

In Section II the details of the full-order modeling, model-order reduction, and transient optimizations are presented. In Section III numerical results are presented which validate the model-order reduction technique through comparisons of full-order and reduced-order open-loop transient responses. This section also presents results demonstrating the potential to increase measures of thermal dose [13] through use of the proposed open-loop transient optimization technique. It is also demonstrated in this section that the feedback controller designed in conjunction with the ROM is capable of tracking the command signal despite abrupt changes in tumor perfusion rates. Section IV summarizes the salient features of the proposed techniques and the results of the numerical experiments.

II. Method

A detailed account of the proposed numerical modeling and optimization procedures for electromagnetic hyperthermia is presented below. Section II-A describes the numerical models that are used to predict the time-dependent temperature rise in the body due to the hyperthermia applicator. Section II-B describes use of the SLDM to produce reduced-order models suitable for efficient evaluation and optimization of transient temperature fields. Lastly, Section II-C describes details of the two proposed transient temperature optimization procedures.

A. Numerical Modeling of the Hyperthermia Process

In typical electromagnetic hyperthermia treatments the time-scale of transient electromagnetic phenomena is orders-of-magnitude smaller than that of thermal phenomena. It is therefore convenient to model the entire hyperthermia process as consisting of two events: the time-harmonic transfer of electromagnetic energy from the antennae of the applicator to the tissue and the resultant time-dependent temperature rise. To describe the process by which the antennae of the hyperthermia applicator deposit heat in the human body, it is assumed that the human body can be accurately modeled as a nonmagnetic, isotropic, linear (but possibly dispersive) electromagnetic material at the frequencies of interest (40-915 MHz). In this frequency range the electromagnetic properties of human tissue are known with a relatively high degree of confidence and have been tabulated in the literature [26], [27]. The finite-difference time-domain (FDTD) method [28] is used in this work to numerically solve for the electric field due to each element of the array under unitary excitation. This procedure has been well documented in the literature [29]–[31], including the current authors' implementation [9], therefore no further detail is provided here.

From knowledge of the electric fields due to the individual elements of the applicator array, the specific absorption rate (SAR) may be predicted. This information can be used to determine optimal relative driving phases and amplitudes of the array in a separate procedure, based on criteria related to the SAR distribution [6], [7] or resultant steady-state temperature [9], [12]. In this work, only patient positioning is used to focus the SAR on the tumor, with the APA elements all driven by equal phases and amplitudes. A recent work [32] has suggested that when it can be done accurately, patient positioning may be the most effective means of focusing SAR patterns on the tumor.

To predict the temperature rise once the SAR is known, some type of thermal model must be assumed. One of the simplest thermal models that can adequately describe the evolution of temperature in biological media is the

bio-heat transfer equation (BHTE) [33] due to Pennes. Although there are many known limitations to the BHTE [2], it remains a popular model for describing temperature rises in human tissue [34], [35]. The transient form of the BHTE is

$$\rho(\boldsymbol{r})c(\boldsymbol{r})\frac{\partial T(\boldsymbol{r},t)}{\partial t} = \nabla\cdot k(\boldsymbol{r})\nabla T(\boldsymbol{r},t) + u(t)\rho(\boldsymbol{r})\mathrm{SAR}(\boldsymbol{r}) + c_b\, w(\boldsymbol{r},T)\,(T_a - T(\boldsymbol{r},t)) + q_m(\boldsymbol{r}) \quad (1)$$

where k is the local thermal conductivity (W/m/K), ρ is the local density of tissue (kg/m^3), c is the local specific heat (J/kg/K), c_b is the specific heat of blood (J/kg/K), w is the local perfusion rate of blood (kg/s/m^3), T_a is the arterial blood temperature (K), q_m is the time rate of metabolic heat generated per unit volume (W/m^3), and $u(t)$ is a dimensionless quantity representing the relative total power deposited. The perfusion rate will be assumed constant with respect to local temperature throughout most of this work so that $w(\boldsymbol{r},T) = w(\boldsymbol{r})$. This is a somewhat unrealistic approximation, and in the simulations of the performance of the feedback controller the effects of relaxing this assumption will be briefly explored.

The boundary conditions associated with the BHTE are

$$k\frac{\partial T(\boldsymbol{r},t)}{\partial n} = H(T_w - T(\boldsymbol{r},t)), \quad \boldsymbol{r}\in S_N \quad (2)$$

$$T(\boldsymbol{r},t) = T_f, \quad \boldsymbol{r}\in S_D \quad (3)$$

where S_N is a surface on which convective heat transfer occurs with coefficient H and external medium temperature T_w, and S_D is a surface of fixed temperature T_f.

The *basal* temperature distribution $T_{\mathrm{basal}}(\boldsymbol{r})$ is that associated with the equilibrial effects of metabolic heat production. The transient temperature elevation, $T_{\mathrm{tr}}(\boldsymbol{r},t)$, is defined as the instantaneous difference of the total temperature field and the basal temperature distribution, i.e. $T_{\mathrm{tr}}(\boldsymbol{r},t) = T(\boldsymbol{r},t) - T_{\mathrm{basal}}(\boldsymbol{r})$. After application of the finite-difference method [35] to discretize the spatial operators in the BHTE, the transient temperature field is approximately described by the following matrix ordinary differential equation

$$\frac{\partial \boldsymbol{x}(t)}{\partial t} = \bar{\boldsymbol{A}}\boldsymbol{x}(t) + \boldsymbol{b}u(t) \quad (4)$$

In the above expression, $\boldsymbol{x}(t)$ is an N-vector of degrees of freedom associated with the discretized temperature field, $\boldsymbol{b}$ is an N-vector associated with deposition of power by the antennae, and $\bar{\boldsymbol{A}}$ is an N-by-N matrix representing the effects of perfusion, conduction and convection.

The zero-state solution of Eq. 4 can be analytically expressed

$$\boldsymbol{x}(t) = \exp\left(\bar{\boldsymbol{A}}t\right) h(t) * \boldsymbol{b}u(t) \quad (5)$$

where $h(t)$ is the Heaviside unit step function and $*$ is the temporal convolution operator. Because of the large size of the matrices involved, it is often not feasible to evaluate Eq. 5 directly. For this reason, it is common to discretize the temporal dependence as well. In this work, when dealing with high-dimensional models (large N), time integration will be achieved through a Crank-Nicolson update rule of the following type

$$\left[\bar{\boldsymbol{I}} - \frac{\Delta t}{2}\bar{\boldsymbol{A}}\right]\boldsymbol{x}(t+\Delta t) = \left[\bar{\boldsymbol{I}} + \frac{\Delta t}{2}\bar{\boldsymbol{A}}\right]\boldsymbol{x}(t) + \frac{\Delta t}{2}\boldsymbol{b}\left[u(t+\Delta t) + u(t)\right] \quad (6)$$

After the application of the model-order reduction technique described below, it will often be feasible to evaluate Eq. 5 directly.

B. The Spectral Lanczos Decomposition Method (SLDM)

The spectral Lanczos decomposition method [23], [24] was originally proposed for efficient evaluation of functionals of large, sparse matrices. Above, Eq. 5 at a fixed time serves as an example of how the computation of a large matrix functional is useful in time-dependent temperature prediction. The most important feature of the SLDM in this work, however, is that a reduced-order model (ROM) results from its application. The lower dimensionality of the ROMs produced will lead to a reduction in computational burden in the optimization techniques to be presented in Section II-C.

B.1 The Lanczos Algorithm

The SLDM is one of the simplest of a class of model-order reduction schemes based on the Lanczos algorithm. An exposition of the theoretical motivation and properties of the Lanczos algorithm appears in [36], so only a brief summary is given here. The Lanczos algorithm, given a N-by-N symmetric matrix $\bar{\boldsymbol{L}}$ and an initial N-vector $\boldsymbol{q}_1$ of unit norm, is defined by the following steps:

- Let $\beta_0\boldsymbol{r}_0 = 0$, $\beta_0 = 1$
- Do for $i \in \{1, 2, \ldots, p\}$
  1. $\alpha_i = \boldsymbol{q}_i^T\bar{\boldsymbol{L}}\boldsymbol{q}_i$
  2. $\boldsymbol{r}_i = \left(\bar{\boldsymbol{L}} - \alpha_i\bar{\boldsymbol{I}}\right)\boldsymbol{q}_i - \beta_{i-1}\boldsymbol{q}_{i-1}$
  3. $\beta_i = \|\boldsymbol{r}_i\|$
  4. $\boldsymbol{q}_{i+1} = \frac{\boldsymbol{r}_i}{\beta_i}$

After these p steps of the Lanczos algorithm, a partial tridiagonalization of the matrix $\bar{\boldsymbol{L}}$ has been achieved which can be expressed

$$\bar{\boldsymbol{L}}\bar{\boldsymbol{Q}}_p = \bar{\boldsymbol{Q}}_p\bar{\boldsymbol{T}}_p + \beta_p\boldsymbol{q}_{p+1}\boldsymbol{e}_p^T \quad (7)$$

where $\boldsymbol{e}_p^T$ is the unit vector composed of all zeroes except a unit entry in the p^{th} position, $\bar{\boldsymbol{Q}}_p$ is the matrix of

Lanczos vectors $\bar{\boldsymbol{Q}}_p = [\boldsymbol{q}_1, \boldsymbol{q}_2, ..., \boldsymbol{q}_p]$, and the tridiagonal matrix $\bar{\boldsymbol{T}}_p$ is given by

$$\bar{\boldsymbol{T}}_p = \begin{bmatrix} \alpha_1 & \beta_1 & & \cdots & 0 \\ \beta_1 & \alpha_2 & \ddots & & \vdots \\ & \ddots & \ddots & \ddots & \\ \vdots & & \ddots & \ddots & \beta_{p-1} \\ 0 & \cdots & & \beta_{p-1} & \alpha_p \end{bmatrix} \tag{8}$$

A key property of the Lanczos algorithm is that the majority of the computational burden at each step is consumed by one matrix-vector multiplication. For sparse matrices such as those resulting from finite-difference approximations, this step can be made very efficient. The eigenvalue spectrum of the tridiagonal matrix $\bar{\boldsymbol{T}}_p$ becomes a very good approximation to that of $\bar{\boldsymbol{L}}$ for $p \ll n$ [36], so the entire p-step Lanczos algorithm can be performed very quickly, even when N is large.

Given a matrix functional of the form $f(\bar{\boldsymbol{L}})\,\boldsymbol{b}$ it is desired to evaluate, the SLDM produces an approximation through performing p steps of the Lanczos procedure with the matrix $\bar{\boldsymbol{L}}$ and starting vector $\boldsymbol{b}/\|\boldsymbol{b}\|$ and taking

$$f(\bar{\boldsymbol{L}})\,\boldsymbol{b} \approx \bar{\boldsymbol{Q}}_p f(\bar{\boldsymbol{T}}_p)\,\boldsymbol{e}_1 \|\boldsymbol{b}\| \tag{9}$$

as the approximate value of the desired function, where $\boldsymbol{e}_1$ is the unit vector with nonzero first row only. The numerical efficiency accomplished by the approximation Eq. 9 is due to the fact that, in practice, $p \ll n$ and the fact that $\bar{\boldsymbol{T}}_p$ is tridiagonal. In this work, the PWK variant of the QR algorithm and the inverse-iteration algorithm [36] are used to perform the complete eigendecomposition of this tridiagonal matrix, facilitating the evaluation of the right side of Eq. 9. It is straightforward to prove that the SLDM approximation embodied by Eq. 9 after p steps is exact for polynomial functions $f(\cdot)$ of degree $p-1$ or less [37]. This implies the following useful fact which will be needed later

$$(\bar{\boldsymbol{L}})^m = \bar{\boldsymbol{Q}}_p\,(\bar{\boldsymbol{T}}_p)^m\,\bar{\boldsymbol{Q}}_p^T, \quad \text{for} \quad m < p-1 \tag{10}$$

B.2 Model-Order Reduction

Use of the SLDM in two different moment-matching model-order reduction techniques [38] is described below. Consider first the general linear time-invariant single-input multiple-output (SIMO) system described by the state-space model

$$\frac{\partial \boldsymbol{x}(t)}{\partial t} = \bar{\boldsymbol{A}}\boldsymbol{x}(t) + \boldsymbol{b}u(t) \tag{11}$$

$$\boldsymbol{y} = \bar{\boldsymbol{C}}\boldsymbol{x} \tag{12}$$

where $\bar{\boldsymbol{C}} \in \mathcal{R}^{M \times N}$ is a matrix which represents the relation between the state vector $\boldsymbol{x}$ and observable measurements $\boldsymbol{y} \in \mathcal{R}^M$. Taking the Laplace transform of all the quantities above and assuming the system is initially at rest yields the following expression of the full-order transfer function

$$\boldsymbol{h}(s) = \boldsymbol{y}(s)/u(s) = \bar{\boldsymbol{C}}\left(s\bar{\boldsymbol{I}} - \bar{\boldsymbol{A}}\right)^{-1}\boldsymbol{b} \tag{13}$$

The Taylor expansion of $\boldsymbol{h}(s)$ about the point $s = 0$ is given by

$$\begin{aligned} \boldsymbol{h}(s) &= -\bar{\boldsymbol{C}}\bar{\boldsymbol{A}}^{-1}\boldsymbol{b} - s\bar{\boldsymbol{C}}\bar{\boldsymbol{A}}^{-2}\boldsymbol{b} + ... - s^{p-1}\bar{\boldsymbol{C}}\bar{\boldsymbol{A}}^{-p}\boldsymbol{b} + ... \\ &= -\sum_{i=0}^{\infty} s^i \bar{\boldsymbol{C}}\bar{\boldsymbol{A}}^{-i-1}\boldsymbol{b} \end{aligned} \tag{14}$$

The tendency of spatially diffusive processes to attenuate input signals of high temporal frequency suggests that the low-frequency behavior of state-space models contain most of the useful information [20]. This information is embedded in the vector moments of the expansion of the transfer function about $s = 0$. With this in mind, the following model-order reduction scheme, termed low-pass SLDM (LPSLDM) is proposed:

1. Begin the Lanczos algorithm with the matrix $\bar{\boldsymbol{A}}^{-1}$ and initial vector $\bar{\boldsymbol{A}}^{-1}\boldsymbol{b}/\|\bar{\boldsymbol{A}}^{-1}\boldsymbol{b}\|$.
2. Continue Lanczos iterations until the quantity $\|\bar{\boldsymbol{C}}\bar{\boldsymbol{Q}}_p\bar{\boldsymbol{T}}_p\left(\exp\left(-\bar{\boldsymbol{T}}_p t_0\right) - \bar{\boldsymbol{I}}\right)\bar{\boldsymbol{Q}}_p^T\bar{\boldsymbol{A}}^{-1}\boldsymbol{b}\|$ converges.

The quantity used in the above stopping criterion represents the output trajectory at time t_0 due to a step input. It will be clear from numerical experiments presented later that t_0 should be chosen as the earliest time of interest. The choice of $\bar{\boldsymbol{A}}^{-1}$ and initial vector $\bar{\boldsymbol{A}}^{-1}\boldsymbol{b}$ can be justified by considering the resulting reduced-order approximation of the transfer function

$$\boldsymbol{h}^{LP}(s) = \bar{\boldsymbol{C}}\bar{\boldsymbol{Q}}_p\left(s\bar{\boldsymbol{I}} - \bar{\boldsymbol{T}}_p^{-1}\right)^{-1}\bar{\boldsymbol{Q}}_p^T\boldsymbol{b} \tag{15}$$

whose moments about $s = 0$ can be expressed, using the fact that the matrix $\bar{\boldsymbol{Q}}_p$ is orthonormal and the identity in Eq. 10,

$$\begin{aligned} \boldsymbol{h}^{LP}(s) &= -\sum_{i=0}^{\infty} s^i \bar{\boldsymbol{C}}\bar{\boldsymbol{Q}}_p\left(\bar{\boldsymbol{T}}_p^{-1}\right)^{i+1}\bar{\boldsymbol{Q}}_p^T\boldsymbol{b} \\ &= -\sum_{i=0}^{p-2} s^i \bar{\boldsymbol{C}}\bar{\boldsymbol{A}}^{-i-1}\boldsymbol{b} + O\left(s^{p-1}\right) \end{aligned} \tag{16}$$

From the above expression, it is clear that the first $p-1$ moments of $\boldsymbol{h}^{LP}(s)$ are identical to those of $\boldsymbol{h}(s)$, suggesting that LPSLDM is a good approximation for low frequency transients. The major drawback of the LPSLDM is that performance of the Lanczos algorithm on $\bar{\boldsymbol{A}}^{-1}$ requires a large linear system be solved at each step. Avoiding this expense is the principal motivation for the next model-order reduction procedure, referred to as the high-pass SLDM (HPSLDM).

To motivate the HPSLDM, consider the Laurent expansion of $\boldsymbol{h}(s)$ about the point $s = \infty$ [38]

$$\begin{aligned}\boldsymbol{h}(s) &= s^{-1}\bar{\boldsymbol{C}}\boldsymbol{b} + s^{-2}\bar{\boldsymbol{C}}\bar{\boldsymbol{A}}\boldsymbol{b} + \ldots + s^{-p}\bar{\boldsymbol{C}}\bar{\boldsymbol{A}}^{p-1}\boldsymbol{b} + \ldots \\ &= \sum_{i=1}^{\infty} s^{-i}\bar{\boldsymbol{C}}\bar{\boldsymbol{A}}^{i-1}\boldsymbol{b} \end{aligned} \tag{17}$$

The high-pass SLDM (HPSLDM) model-order reduction used in this work is accomplished by the following steps:

1. Begin the Lanczos algorithm with the matrix $\bar{\boldsymbol{A}}$ and initial vector $\boldsymbol{b}/\|\boldsymbol{b}\|$.
2. Continue Lanczos iterations until the quantity $\|\bar{\boldsymbol{C}}\bar{\boldsymbol{Q}}_p\bar{\boldsymbol{T}}_p^{-1}\left(\exp\left(\bar{\boldsymbol{T}}_p t_f\right) - \bar{\boldsymbol{I}}\right)\bar{\boldsymbol{Q}}_p^T\boldsymbol{b}\|$ converges.

The quantity used in the above stopping tolerance represents the output trajectory at time t_f due to a step input which, as numerical experiment will show, should be chosen as the *latest* time of interest, in contrast to the use of the *earliest* time of interest for the LPSLDM. The choice of $\bar{\boldsymbol{A}}$ and initial vector $\boldsymbol{b}$ can again be justified by noting that the first p moments of the transfer function about $s = \infty$ are indentical for the HPSLDM and full-order models (the proof is similar to that provided for the LPSLDM). However, this suggests that this is a good approximation for fast transients only, which is not clearly desirable for approximating the low-pass nature of heat transfer. The advantage of the HPSLDM is that it requires only a series of matrix-vector products, in contrast to the LPSLDM which requires a series of solutions to linear systems. However, it will be shown that given large enough p, the HPSLDM can produce accurate reduced-order models.

C. Transient Temperature Optimization

Approaches for optimization of hyperthermia temperature fields can be broadly classified into two main categories: open-loop and closed-loop. Open-loop techniques [4], [6], [9], [12] use a physical model of the hyperthermia process to determine optimal treatment parameters. The most significant disadvantage to this approach is that the optimization may be very sensitive to modeling errors. Closed-loop techniques [18], [34] attempt to rectify this through use of measurements of treatment temperatures to adjust optimal parameters.

Below, the details of two techniques for transient temperature optimization in hyperthermia are presented. The first is an open-loop technique which attempts to minimize the difference between the desired and realized intratumoral temperature trajectories. The major advantage of this technique is that it can guarantee the temperature at a finite set of extratumoral points will not exceed a given threshold if the underlying model is accurate. Additionally, it can explicitly account for available power limitations. The second technique is a closed-loop technique based on linear-quadratic control [39]. The feedback controller that results from this technique uses measurements of temperatures in the tumor to attempt to compensate for modeling errors.

C.1 Open-Loop Formulation: Quadratic Programming

Examples of open-loop techniques applied to hyperthermia temperature control in the literature include quadratic and min-max techniques [14], [15], indirect use of the maximum principle of Pontryagin [16], and direct inversion of the BHTE [40]. Application of the maximum principle of Pontryagin leads to a *bang-bang* controller, which in general switches up to $n-1$ times when controlling a plant of dimension n with all real nondefective eigenvalues. However, the technique proposed in [16] assumes that the optimal switching profile contains only one switch, which is not generally true. Direct inversion of the BHTE as in [40] is only feasible when pointwise prescription of the power deposition pattern in space is possible. Neither of these limitations are associated with the approach of [14], [15].

In this work, a formulation similar to that presented in [14] is pursued to illustrate the application of reduced-order modeling. It is desired to determine the time-history of RF input power $u(t)$ that minimizes the time-integrated sum of squared differences between desired temperature elevations and realized temperature elevations at a finite number of points. At the same time, it is required that the temperature elevation at a number of points in the healthy tissue remain below a threshold temperature at all times.

These goals can be expressed mathematically as

$$\text{minimize } J(u) = \int_0^{t_f} \|\bar{\boldsymbol{C}}_t\boldsymbol{x}(t) - \boldsymbol{y}_c^*(t)\|^2 dt \tag{18}$$

$$\text{subject to } \bar{\boldsymbol{C}}_h\boldsymbol{x}(t) \le \boldsymbol{y}_p^*(t) \tag{19}$$

$$\frac{\partial \boldsymbol{x}(t)}{\partial t} = \bar{\boldsymbol{A}}\boldsymbol{x}(t) + \boldsymbol{b}u(t) \tag{20}$$

$$u(t) \in \mathcal{U} \tag{21}$$

where $J(u)$ is the scalar cost of the input waveform, determined in terms of the desired temperature elevation history at N_t points in space $\boldsymbol{y}_c^*(t) \in \mathcal{R}^{N_t}$ and the realized temperature, which is calculated by multiplying the realized state $\boldsymbol{x}(t)$ with the matrix $\bar{\boldsymbol{C}}_t \in \mathcal{R}^{N_t \times N}$. This cost is minimized while keeping the temperature at N_h points in healthy tissue (calculated by multiplying the matrix $\bar{\boldsymbol{C}}_h \in \mathcal{R}^{N_h \times N}$ by the temperature elevation history) below a set of threshold values $\boldsymbol{y}_p^*(t) \in \mathcal{R}^{N_h}$. The restriction $u(t) \in \mathcal{U}$ means that the resultant power waveform is realizable. For example, the input power must always be non-negative and is frequently limited in practice by the available power of the RF source.

To recast the above problem into a form suitable for computer implementation, the input waveform is first discretized

$$u(t) = \sum_{i=1}^{N_u} \alpha_i n_i(t) \tag{22}$$

so that given the set of basis functions $n_i(t)$, the input is completely characterized by the set of parameters $\boldsymbol{u} = [\alpha_1, \alpha_2, \ldots, \alpha_{N_u}]^T$. In this work, a piecewise constant input profile is assumed, with the basis functions

$$n_i(t) = h(t - t_i) - h(t - t_{i-1}) \tag{23}$$

where t_i are a set of switching times. The requirement that the input power be non-negative and not exceed the maximum available power is then captured by the requirements $0 \leq \alpha_i \leq U_{\max}$.

The temperature elevation can then be expressed

$$\begin{aligned} \boldsymbol{x}(t) &= \sum_{i=1}^{N_u} \alpha_i \exp\left(\bar{\boldsymbol{A}}t\right) h(t) * n_i(t)\boldsymbol{b} \\ &= \sum_{i=1}^{N_u} \alpha_i \hat{\boldsymbol{n}}_i(t) = \bar{\boldsymbol{N}}(t)\boldsymbol{u} \end{aligned} \tag{24}$$

where $\bar{\boldsymbol{N}}(t) = [\hat{\boldsymbol{n}}_1(t), \hat{\boldsymbol{n}}_2(t), \ldots, \hat{\boldsymbol{n}}_{N_u}(t)]^T$. The only remaining difficulty is the enforcement of the protection of healthy tissue at all times. However, if we choose to only enforce this explicitly at a finite number of times, then a finite set of inequalities result

$$\bar{\boldsymbol{C}}_h \boldsymbol{x}(t_j) \leq \boldsymbol{y}_p^*(t_j) \quad j = 1, \ldots, N_c \tag{25}$$

The resulting finite quadratic program can be expressed (where the constant part of the cost has been removed),

$$\text{minimize } \boldsymbol{u}^T \bar{\boldsymbol{H}} \boldsymbol{u} + \boldsymbol{g}^T \boldsymbol{u} \tag{26}$$

$$\text{subject to } \bar{\boldsymbol{C}}_h \bar{\boldsymbol{N}}(t_j)\boldsymbol{u} \leq \boldsymbol{y}_p^*(t_j) \quad j = 1, \ldots, N_c \tag{27}$$

$$0 \leq \alpha_i \leq U_{\max} \quad i = 1, \ldots, N_u \tag{28}$$

where the elements of the matrix $\bar{\boldsymbol{H}}$ and vector $\boldsymbol{f}$ are given by

$$H_{ij} = \int_0^{t_f} \left(\bar{\boldsymbol{C}}_t \hat{\boldsymbol{n}}_i(t)\right)^T \left(\bar{\boldsymbol{C}}_h \hat{\boldsymbol{n}}_j(t)\right) dt \tag{29}$$

$$f_i = -\int_0^{t_f} \boldsymbol{y}_p^*(t) \bar{\boldsymbol{C}}_t \hat{\boldsymbol{n}}_i(t) dt \tag{30}$$

The integrations required in the above are carried out numerically via Romberg integration. A reduced-order model obtained from the SLDM is employed to evaluate the quantities $\hat{\boldsymbol{n}}_i(t)$ as needed. To use the full-order model of the dynamics would require either repeated re-evaluation of the temperature fields or storage of the temperature history due to each of the basis functions. Although it is possible to minimize the computational burden of the latter approach by storing only one step response and exploiting the time-invariance of the system to form the responses from each basis function *on the fly*, this approach is not pursued here. To retain the focus of this work on the suitability of Lanczos-type model-order reduction, computation of a minimum that achieves some clinical objective will be considered a successful use of the ROM. Once the ROM is employed, the resulting quadratic program may be solved using a number of techniques [41]. In this work, the MATLAB© (The Mathworks Inc., Natick, MA, version 5.3 release 11) command *qp* is used to numerically solve the program.

C.2 Closed-Loop Formulation: Linear-Quadratic Control

Uncertainties in constitutive parameters, patient positioning, and perfusion profiles make the use of open-loop treatment optimization potentially ineffective. This difficulty can be overcome to some extent by using a closed-loop controller which uses measurements in addition to a model of the system to achieve its goal. Linear-quadratic (LQ) control and estimation have been applied in the past to hyperthermia controller design [18], [19]. In [18] the use of reduced-order models for optimal servomechanism [39] controller design was proposed and validated via comparison with full-order controllers. The requirement that temperatures at all locations in the state-space model be measurable was removed in [19] through use of a Kalman filter. The issue of removing "integrator wind-up," a problem related to the non-negativity of power, has also been addressed for the case of multiple incoherent radiators in [42].

A recent development which makes the use of non-invasive temperature monitoring clinically possible during hyperthermia treatments is the emergence of MRI-based thermography [34]. The characteristics of MRI thermography, which are significantly different from those of traditional invasive temperature probes, demand special attention when designing a control scheme. MRI thermograms usually contain spatially dense (a complete axial slice at near millimeter resolution) which is updated rather infrequently (2-3 times a minute) due to the inherently low signal-to-noise ratio of MRI.

In this section, the approach of [19] is extended to the case when MRI thermograms are the source of temperature feedback and phased-arrays are the source of heating. The emphasis of the current investigation is the ability of the resulting optimal servomechanism controller with Kalman estimator to control and estimate temperatures reliably in the presence of noise, sparse temporal information, and changes in tumor perfusion rates.

In coherent multi-applicator heating systems (as in electromagnetic APA hyperthermia), the individual phases and amplitudes of each channel have a non-linear influence on the temperature field. For simplicity therefore, the only quantity to be controlled in this work is the RF input power level, again denoted $u(t)$, whose effect on the temperature is linear (assuming the thermal dynamics are linear as well). Additionally, it is attempted to drive only one scalar quantity to a desired value. This may be a temperature at a single point or a linear function of temperatures at different points, such as the average tumor temperature.

Denoting the temperature to be controlled $y(t) = \bar{C}_1 \boldsymbol{x}(t)$ and its desired value y^*, a consistent goal is to attempt to drive the state to the value $\boldsymbol{x}^* = \bar{C}_1^T \left(\bar{C}_1 \bar{C}_1^T\right)^{-1} y^*$. The difference between the realized state and desired state is then defined, $\delta\boldsymbol{x}(t) = \boldsymbol{x}(t) - \boldsymbol{x}^*$, which can be shown to obey affine dynamics of the form

$$\frac{d\delta\boldsymbol{x}(t)}{dt} = \bar{\boldsymbol{A}}\delta\boldsymbol{x}(t) + \boldsymbol{b}u(t) + \boldsymbol{w} \tag{31}$$

where the term $\boldsymbol{w} = \bar{\boldsymbol{A}}\boldsymbol{x}^*$ appears due to the tracking nature of the problem.

Since the measurements will not be available in continuous time, the entire system can be integrated under the assumption that the control signal is held at a constant level between measurement times. Additionally, once the control difference is defined as $v[k+1] = u[k+1] - u[k]$ and the state error difference is defined as $\delta\boldsymbol{x}_d[k+1] = \delta\boldsymbol{x}[k+1] - \delta\boldsymbol{x}[k]$, the full system dynamics can be expressed

$$\begin{pmatrix} \delta\boldsymbol{x}_d \\ \bar{C}_1\delta\boldsymbol{x} \end{pmatrix}[k+1] = \begin{pmatrix} \bar{\boldsymbol{\mathcal{A}}} & \bar{\boldsymbol{0}} \\ \bar{C}_1\bar{\boldsymbol{\mathcal{A}}} & \bar{I} \end{pmatrix} \begin{pmatrix} \delta\boldsymbol{x}_d \\ \bar{C}_1\delta\boldsymbol{x} \end{pmatrix}[k] + \begin{pmatrix} \hat{\boldsymbol{b}} \\ \bar{C}_1\hat{\boldsymbol{b}} \end{pmatrix} v[k] \tag{32}$$

where the new system matrix $\bar{\boldsymbol{\mathcal{A}}} = \exp\left(\bar{\boldsymbol{A}}\Delta t\right)$ and forcing vector $\hat{\boldsymbol{b}} = \bar{\boldsymbol{A}}^{-1}\left[\exp\left(\bar{\boldsymbol{A}}\Delta t\right) - \bar{I}\right]\boldsymbol{b}$ can be computed, in principle, from knowledge of the measurement interval Δt and the continuous time models. The reason for formulating the system as in Eq. 32 is to identify a *linear* (as opposed to affine) system which possesses a state which is composed of quantities which are desired to be driven to zero. In this way, standard linear-quadratic *regulator* techniques can be used to achieve *tracking* of the desired temperature.

Applying standard LQR theory [39] to the cost

$$J(v) = \sum_{k=0}^{\infty} \left(\delta\boldsymbol{x}^T[k]\bar{C}_1^T\bar{C}_1\delta\boldsymbol{x}[k] + v[k]\rho v[k]\right) \tag{33}$$

with $\rho > 0$ results in a set of gains $\bar{\boldsymbol{K}}_1$ and $\bar{\boldsymbol{K}}_2$ which describe the optimal servomechanism control law

$$u[k] = -\bar{\boldsymbol{K}}_1\delta\boldsymbol{x}[k] - \bar{\boldsymbol{K}}_2 \sum_{i=0}^{\infty} \bar{C}_1\delta\boldsymbol{x}[i] \tag{34}$$

This control can be shown to minimize the cost in Eq. 33. If it happens in the course of a treatment that the recommended control is negative, the summation in Eq. 34 can be set to zero and no power applied until the recommended control is once again positive. In this way, "wind-up" of the summation is prevented.

As illustrated by Eq. 34, knowledge of the entire state is required to compute the optimal control. To estimate the state from the limited available measurements, an observer must be implemented. A fortunate characteristic of linear-quadratic control is that the design of the estimator can be done in isolation from that of the controller, a fact known widely as the "certainty equivalence" principle [39]. In accordance with this principle, Eq. 34 is used as the control law, substituting the *estimate* $\delta\hat{\boldsymbol{x}}[k]$ of the current state, which is obtained as the output of the *observer*

$$\hat{\boldsymbol{x}}[k+1] = \bar{\boldsymbol{\mathcal{A}}}\hat{\boldsymbol{x}}[k] + \hat{\boldsymbol{b}}u[k] + \bar{\boldsymbol{\mathcal{M}}}\left(\boldsymbol{y}_{\text{meas}}[k] - \bar{C}_{\text{meas}}\hat{\boldsymbol{x}}[k]\right) \tag{35}$$

where $\boldsymbol{y}_{\text{meas}}[k]$ is the set of N_m measurements available at each time step, $\bar{C}_{\text{meas}}$ is a matrix used to calculate the estimate of the what the measurement should be if the state estimate is correct. The matrix $\bar{\boldsymbol{\mathcal{M}}}$ is the so-called Kalman gain, obtained from solution of the relevant Ricatti equation involving the correlations of the state and measurement noise. More detail on the Kalman filter (optimal observer) can be found in [19], [39]. In our implementation, we assume that the correlation of the measurement noise vector is diagonal with value $\sigma_{\text{meas}}\bar{I}$ which is computed based on the expected noise level of the system. The state noise correlation is also assumed diagonal $\sigma_{\text{state}}\bar{I}$ which is chosen based on the uncertainty in perfusion values.

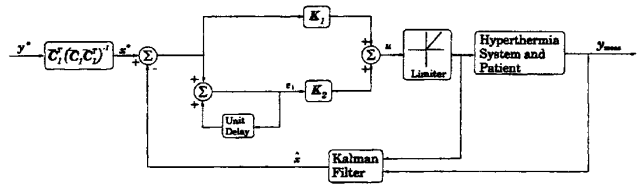

Fig. 1. Structure of the optimal controller and estimator. The integrated error e_i is reset to zero when the limiter is active.

The numerical determination of the Kalman and control gains involves the solution of Ricatti equations, which is difficult to perform in an efficient and stable fashion when the state-space system has large dimension [18].

For this reason, a reduced-order model obtained from the LPSLDM is used instead of the original model

$$\frac{d\boldsymbol{x}^{\mathrm{ROM}}}{dt} = \bar{\boldsymbol{Q}}_p^T \frac{d\boldsymbol{x}}{dt} = \bar{\boldsymbol{T}}_p^{-1} \bar{\boldsymbol{Q}}_p^T \boldsymbol{x} + \bar{\boldsymbol{Q}}_p^T \boldsymbol{b} u(t) = \bar{\boldsymbol{T}}_p^{-1} \boldsymbol{x}^{\mathrm{ROM}} + \bar{\boldsymbol{Q}}_p^T \boldsymbol{b} u(t) \quad (36)$$

and the change of basis $\boldsymbol{x}^{\mathrm{ROM}} = \bar{\boldsymbol{Q}}_p^T \boldsymbol{x}$ used to express all of the equations in this section in terms of the ROM state. The LPSLDM ROM is selected because it is generally of lower dimension than the HPSLDM ROM. The MATLAB© (The Mathworks Inc., Natick, MA, version 5.3 release 11) routines *dlqr* and *dlqe* are then used to numerically determine the optimal control law and estimator, respectively. The resulting controller-estimator structure is depicted in Figure 1.

III. Results

The techniques elucidated in the above section have been implemented and applied to several simulated examples. Section III-A describes a simple example which serves to validate the SLDM technique by comparing full-order and reduced-order model predictions. Simulated hyperthermia treatment of a phantom is considered in Section III-B and of an anatomically detailed human trunk in Section III-C. The relative merits of the LPSLDM and HPSLDM are explored in terms of their efficiencies as temperature prediction techniques. Additionally, examples of the use of reduced-order models in both open-loop and closed-loop optimization schemes are given.

A. Validation of the SLDM

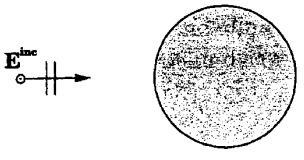

Fig. 2. Geometry assumed for validation of the numerical algorithms. An infinitely long muscle-like cylinder is irradiated by an electromagnetic plane-wave at 85 MHz.

In order to validate the SLDM-based model-order reduction techniques, the exposure of a cylinder of muscle-like material ($\epsilon_r = 78.5$, $\sigma = 0.486\ \Omega^{-1}\mathrm{m}^{-1}$, $\rho = 1070$ kg/m^3, $c = 3140$ Ws/kg/K, $k = 0.502$ W/m/K, $q_m = 1005$ W/m^3, $T_a = 37$°C, $c_b w = 1674$ W/K/m^3) to an electromagnetic plane wave of frequency 85 MHz with an electric field polarized along the axis of the cylinder has been considered (see Figure 2). An incident electromagnetic power density of 0.75 W/cm^2 was applied as a Heaviside step function in time. The cylinder considered had a radius of 25 cm and length of 52 cm, and exchanged heat with an external medium at 24°C with convection coefficient $H = 45$ W/m^2/K. The upper and lower surfaces of the cylinder were assumed to have a uniform, fixed temperature of 37°C.

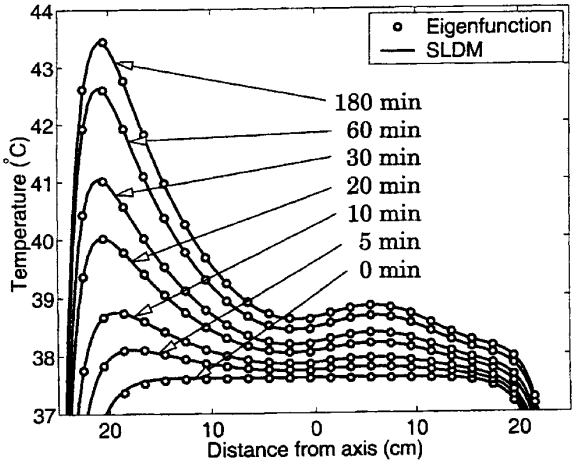

Fig. 3. Predicted temperature fields along central chord of cylinder parallel to the direction of propagation of the incident plane wave.

Figure 3 shows the transient temperature field obtained through three different methods. The first method employed an exact solution to Maxwell's equations for TE-incidence on an infinitely-long cylinder and the eigenfunction method described in [43] to compute the resultant temperature field (again for an infinitely long cylinder). The HPSLDM was also used in conjunction with the FDTD electromagnetic model and FD model of the BHTE to predict the temperature field. The latest time of interest was 180 minutes, at which time 38 HPSLDM modes were required to produce a prediction which converged to within 10^{-4} in norm. Similarly, at the earliest time of interest (5 minutes), 16 LPSLDM modes were required for the prediction to converge. The FDTD and FDM models that the SLDM was applied to were three-dimensional models, with a resolution of 0.5 cm in the transverse plane and 4 cm in the axial direction resulting in 101985 thermal unknowns. Notice that the agreement is good at both early and late times for both the LPSLDM and HPSLDM.

B. Phantom Heating

To demonstrate the use of the proposed model-order reduction techniques on inhomogeneous media the heating of an artificial phantom, similar to that proposed in [12], has been considered. It is composed of three distinct tissue-equivalent materials: muscle, fat, and tumor, whose assumed electromagnetic [27] and thermal [44] properties are summarized in Table I, expressed in standard SI units (cf. Section II-A). A region offset in

TABLE I
THERMAL AND ELECTROMAGNETIC (135 MHz) PROPERTIES OF PHANTOM MATERIALS.

Tissue	k	ρ	c	w_b	ϵ_r	σ
Tumor	0.210	900	3500	0.54	80.0	0.70
Muscle	0.642	1000	3500	2.30	63.5	0.74
Fat	0.642	1000	3500	0.83	12.3	0.07

the axial plane is designated as tumor tissue, as shown in Figure 4. The phantom is assumed to be irradiated by an APA consisting of a set of 8 half-wave dipoles arranged in a circumferential array of diameter 21 cm operating at 135 MHz. All eight elements of the APA are driven with equal phases and amplitudes, so the central axis of the phantom is shifted by 1 cm to help localize heating in the tumor region [12].

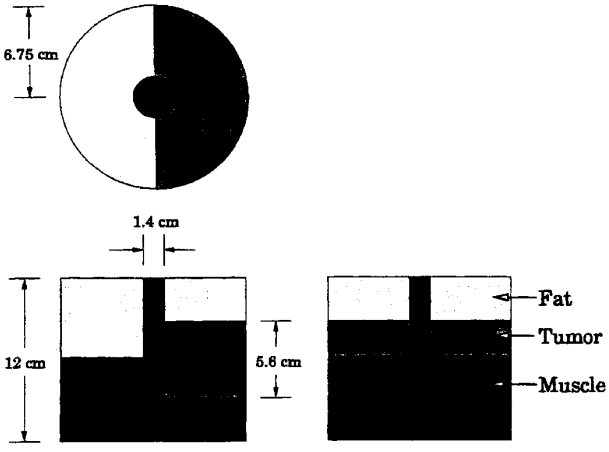

Fig. 4. Orthographic projections of the phantom.

To illustrate the properties of the LPSLDM and HPSLDM as techniques for temperature prediction, the number of Lanczos iterations and CPU time required to reach an error (relative to the Crank-Nicolson prediction) of 10^{-8} in the norm has been considered. An FDM model of the BHTE with uniform resolution of 3.3 mm was used, which resulted in 48285 thermal unknowns. Figure 5 shows that for the HPSLDM, the number of Lanczos iterations required to reach an error level of 10^{-8} always increases as the time of interest increases. However, for the LPSLDM, the number of Lanczos iterations required usually decreases as the time of interest increases. This implies that the order of the ROM should be chosen based on the earliest time of interest for HPSLDM and on the latest time of interest for LPSLDM. Also shown in Figure 5 are the corresponding CPU times on a 500 MHz 21164 DEC Alpha required to perform the needed Lanczos iterations. It is noted that although the LPSLDM generally produces an accurate model with fewer iterations, the CPU time required is similar due to the matrix inversion required at each step, which is performed in this work via the bi-conjugate gradient (BiCG) method.

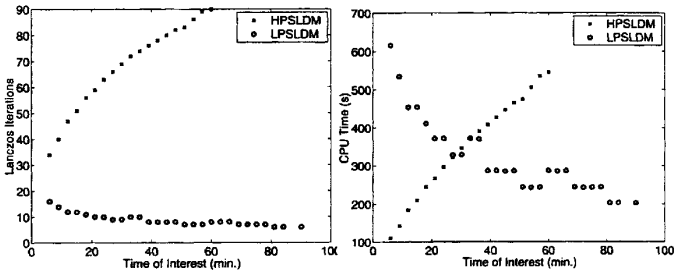

(a) (b)

Fig. 5. Number of Lanczos iterations (a) and CPU time (b) required to produce an estimate of the entire temperature field at a fixed time of interest for the HPSLDM and LPSLDM.

To further explore the merits of SLDM as a temperature prediction technique, the computational burden of predicting the temperature at a fixed time has been examined. The standard for comparison was integration of the full-order model via a Crank-Nicolson update procedure as in Eq. 6 at 5 times the Courant time step for the equivalent Euler integration scheme. This required 150.9 CPU seconds on a 21164 500 MHz Alpha to compute the step response of the temperature at a final time of interest of 2 hours. For the HPSLDM estimate of the step response to converge to within 10^{-6} from step-to-step at a final time of interest of 2 hours, 29 Lanczos steps were required. The Lanczos process required 4.9 CPU sec, and subsequent evaluation of the temperature field at other times required less than 0.1 CPU sec on average. For the LPSLDM estimate of the step response to converge to within 10^{-6} from step-to-step at an earliest time of interest of 5 minutes, only 6 Lanczos steps were required. However, the time required to perform the Lanczos process rose to 37.9 CPU sec, with the average time required to evaluate the temperature at additional times less than 0.05 CPU sec. It can be seen that the lower-order model produced by the LPSLDM comes at the expense of more setup time, suggesting that it is more suitable than HPSLDM only when minimal model-order is the highest priority. In this particular case, the HPSLDM achieved a computational speed up of over 100 relative to the Crank-Nicolson technique.

C. Human Trunk Model

In addition to the inhomogeneous phantom, the simulated heating of a human trunk by an electromagnetic APA has also been considered. The model used for the human trunk is depicted in Figure 6, where the assumed

TABLE II
THERMAL AND ELECTROMAGNETIC (85 MHz) PROPERTIES OF HUMAN TISSUE.

Tissue	k	ρ	c	w_b	ϵ_r	σ
Bladder	0.600	1000	3500	0.80	23.3	0.29
Bone	0.436	1600	1000	0.54	6.7	0.02
Fat	0.210	900	3500	0.54	12.9	0.07
Intestine	0.550	1000	3500	3.33	85.9	0.66
Kidney	0.577	1000	3500	66.7	104.7	0.78
Liver	0.640	1000	3500	16.7	72.7	0.47
Muscle	0.642	1000	3500	2.30	68.0	0.72
Skin	0.293	940	3500	0.35	79.0	0.47
Tumor	0.642	1000	3500	1.80	79.0	0.65

region of the tumor is in the bladder region and is indicated by the honeycomb pattern. The model is based on anatomical phantoms described in [45], and has uniform resolution of 3.4 mm, which resulted in 523233 thermal unknowns after application of the FDM to the BHTE. In this work, nine distinct tissue types were considered, the properties of which [27], [29], [44], [46] are summarized in Table II, expressed in standard SI units (cf. Section II-A). The APA that heats the trunk is modeled as consisting of a set of 8 half-wave dipoles arranged in a circumferential array of diameter 29 cm operating at 85 MHz [5].

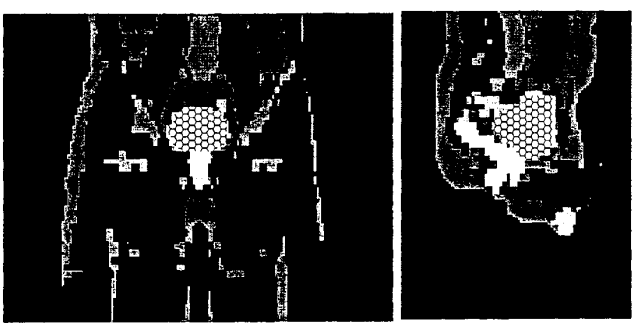

Fig. 6. Coronal and sagittal views of the model of the human trunk. The large, central tumor region is indicated by the honeycombed shading.

As in the case of the phantom, the computational burden of predicting the temperature at a fixed time has been examined. The standard for comparison is again integration of the full-order model via a Crank-Nicolson update at 5 times the Courant step for the equivalent Euler integration scheme. This required 1531.5 CPU seconds on a 21264 500 MHz Alpha to compute the step response of the temperature at a final time of interest of 2 hours. For the HPSLDM estimate of the step response to converge to within 10^{-6} in the norm from step-to-step at a final time of interest of 2 hours, 41 Lanczos steps were required. The Lanczos process required 46.8 CPU sec, and subsequent evaluation of the temperature field at other times required less than 0.8 CPU sec on average. For the LPSLDM estimate of the step response to converge to within 10^{-6} from step-to-step at an earliest time of interest of 5 minutes, only 10 Lanczos steps were required. However, the time required to perform the Lanczos process rose to 432.6 CPU sec, with the subsequent time required to evaluate the temperature at additional times less than 0.25 CPU sec on average. One interesting feature of these results is that even though the number of unknowns is an order-of-magnitude greater than in the case of the phantom, the number of Lanczos steps required for HPSLDM and LPSLDM does not increase much. Additionally, it can be seen that a 30-fold speed-up relative to Crank-Nicolson in computation time is possible via HPSLDM for this particular case.

Figure 7 depicts the results of the open-loop optimization technique applied to the heating of the human trunk model. Twenty-seven points in the tissue positioned inside the tumor and near the outside of the tumor boundary were used in the optimization. A target trajectory of a 12.5 minute ramp-up to 43°C at all points in the tumor was used. Temperatures in the healthy tissue were constrained to remain strictly less than 41°C at the points selected. The LPSLDM ROM described above was used to formulate the quadratic program. In "Case 1," the available RF power was considered as unlimited. In "Case 2," it was assumed that 450 W maximum power was available. Figure 7 (b) depicts the temperature histories, simulated using the full-order model, at the points selected in healthy tissue. It is clear that the constraint is respected. Figure 7 (c) shows the increased speed with which T_{90} and T_{50} (temperatures which are exceeded by 90% and 50% of the tumor, respectively [13]) can be brought to their steady values in both cases relative to the"baseline" (constant power) case.

The full-order model has also been used to simulate the performance of the proposed closed-loop controller. It was desired that the center of mass of the tumor stay at a constant temperature of 44°C. Temperature feedback was assumed to be available from everywhere in the axial midplane of the tumor with a time resolution of 30 sec corrupted by additivie white noise of standard deviation of 0.3°C. The LPSLDM ROM described above was used to design the Kalman filter and linear quadratic regulator. Figure 8 depicts the resulting true and noise-corrupted temperatures at the center of the tumor. Two cases have again been considered, one in which the tumor perfusion is constant at its nominal value of 1.8 (kg/s/m^3) and the other in which the tumor experiences a sudden drop in perfusion to 1.08 (kg/s/m^3) 90 minutes into the treatment. This represents a very simplified model of the temperature-dependent perfusion thought to occur during hyperthermia treatments [44]. It can be seen that

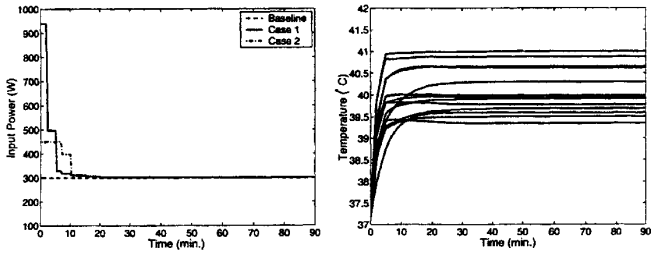

(a) (b)

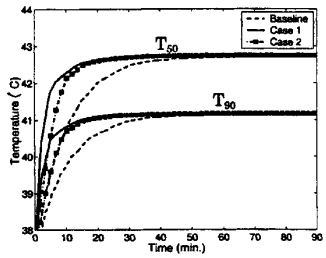

(c)

Fig. 7. Simulated full-order results of open-loop optimization applied to heating of the human trunk model. (a) Returned control trajectories for the baseline and two optimized cases. (b) Temperature trajectories at various points in protected tissues. (c) T_{50} and T_{90} for the baseline and two optimized cases. See text for discussion.

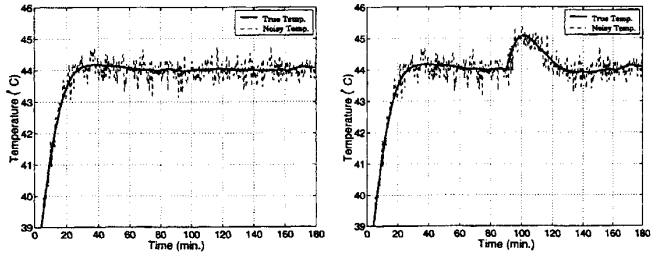

(a) (b)

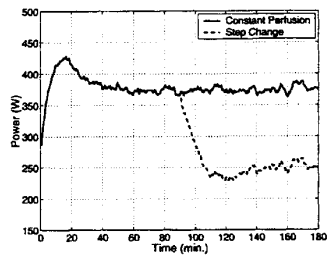

(c)

Fig. 8. Simulated temperature in the center of mass of the human trunk tumor while heated by closed-loop control under (a) constant perfusion and (b) a sudden reduction of 40 % in perfusion in the tumor at 90 minutes. (c) History of the applied input power for both cases.

although this results in temporary overshoot of the temperature in the tumor, the controller adjusts the power to regain tracking of 44°C. A detailed discussion of choices for the reference signal and other tuning and noise sensitivity issues appears in [34]. This example serves to simply demonstrate the feasibility of controller design with Lanczos-based ROMs.

IV. Conclusions

This work examined a model-order reduction technique suitable for large-scale numerical models of biological heating. Two variants of the proposed technique have been presented: one suitable for minimal expense when integrating the system dynamics once (HPSLDM), and the other designed to yield a ROM of minimal dimension (LPSLDM). The use of the resulting ROMs for dynamic optimization of electromagnetic hyperthermia has been demonstrated. Results of the simulated treatments suggest that the effective thermal dose delivered during a fixed treatment time can be maximized while protecting healthy tissue. Additionally, results of the simulated treatments suggest that linear feedback controller designed via the ROMs is capable of compensating for sudden changes in tumor perfusion rates.

V. Acknowledgments

Thanks go to Dr. I. George Zubal of the Yale School of Medicine for generously providing the human trunk model used in this work. The model was developed as a collaboration between Dr. Zubal and Professor Maria A. Stuchly of the University of Victoria.

References

[1] J. Overgaard, D. Gonzalez, M. Hulshof, G. Arcangeli, O. Dahl, O. Mella, and S. Bentzen, "Randomized trial of hyperthermia as an adjuvant to radiotherapy for recurrent or metastatic malignant melanoma," *Lancet*, vol. 345, pp. 540–543, 1995.

[2] R. B. Roemer, "Engineering aspects of hyperthermia therapy," in *Annual Review of Biomedical Engineering*, vol. 1, pp. 347-376, 1999.

[3] P. Wust, M. Seebass, J. Nadobny, P. Deuflhard, G. Monich, and R. Felix, "Simulation studies promote technological development of radiofrequency phased array hyperthermia," *Int. J. Hyperthermia*, vol. 12, no. 4, pp 477–494, 1996.

[4] D. M. Sullivan, "Mathematical methods for treatment planning in deep regional hyperthermia," *IEEE Trans. Microwave Theory Tech.*, vol. 39, no. 5, pp. 864–872, May 1991.

[5] P. F. Turner, "Regional hyperthermia with an annular phased array," *IEEE Trans. Biomed. Eng.*, vol. 31, pp. 106–114, January 1984.

[6] P. Wust, J. Nadobny, R. Felix, P. Deuflhard, A. Louis, and W. John, "Strategies for optimized application of annular-phased-array systems in clinical hyperthermia," *Int. J. Hyperthermia*, vol. 7, no. 1, pp 157–173, 1991.

[7] F. Bardati, A. Borrani, A. Gerardino, and G. A. Lovisolo, "SAR optimization in a phased array radiofrequency hyper-

thermia system," *IEEE Trans. Biomed. Eng.*, vol. 42, no. 12, pp. 1201–1207, December 1995.

[8] K. S. Nikita, N. G. Maratos, and N. K. Uzunoglu, "Optimization of the deposited power distribution inside a layered lossy medium irradiated by a coupled system of concentrically placed waveguide applicators," *IEEE Trans. Biomed. Eng.*, vol. 45, no. 7, pp. 909–920, July 1998.

[9] M. E. Kowalski and J. M. Jin, "Determination of electromagnetic phased array driving signals for hyperthermia based on a steady-state temperature criterion," *IEEE Trans. Microwave Theory Tech.*, vol. 48, no. 11, pp. 1964–1873, Nov. 2000.

[10] K. S. Nikita, N. G. Maratos, and N. K. Uzunoglu, "Optimal steady-state temperature distribution for a phased array hyperthermia system," *IEEE Trans. Biomed. Eng.*, vol. 40, no. 12, pp. 1299–1306, December 1993.

[11] M. Mattingly, R. B. Roemer, and S. Devasia, "Optimal actuator placement for large scale systems: a reduced-order modeling approach," *Int. J. Hyperthermia*, vol. 14, no. 4, pp. 331-345, 1998.

[12] S. K. Das, S. T. Clegg, and T. V. Samulski, "Computational techniques for fast hyperthermia temperature optimization," *Med. Phys.*, vol. 26, no. 2, pp. 319-328, February 1999.

[13] J. R. Oleson, T. V. Samulski, K. A. Leopold, S. T. Clegg, M. W. Dewhirst, R. K. Dodge, and S. L. George, "Sensitivity of hyperthermia trial outcomes to temperature and time: Implications for thermal goals of treatment," *Int. J. Radiation Oncology Biol. Phys.*, vol. 25, pp. 289-297, 1993.

[14] C. De Wagter, "Computer simulation for local temperature control during microwave-induced hyperthermia," *J. Microwave Power*, vol. 20, no. 1, pp. 31-42, January 1985.

[15] C. De Wagter, "Optimization of simulated two-dimensional temperature distributions induced by multiple electromagnetic applicators," *IEEE Trans. Microwave Theory Tech.*, vol. MTT-34, no. 5, pp. 589-596, May 1986.

[16] P. K. Dhar and D. K. Sinha, "Optimal temperature control in hyperthermia by artificial surface cooling," *Int. J. Systems Sci.*, vol. 20, no. 11, pp. 2275-2282, 1989.

[17] J. J. W. Lagendijk, G. C. van Rhoon, S. N. Hornsleth, P. Wust, A. C. C. de Leeuw, C. J. Schneider, J. D. P. van Dijk, J. van der Zee, R. van Heek-Romanowski, S. A. Rahman, and C. Gromoll, "ESHO quallity assurance guidelines for regional hyperthermia," *Int. J. Hyperthermia*, vol. 14, no. 2, pp. 1225-133, 1998.

[18] J. K. Potocki and H. S. Tharp, "Reduced-order modeling for hyperthermia control," *IEEE Trans. Biomed. Eng.*, vol. 39, no. 12, pp. 1265-1273, December 1992.

[19] J. K. Potocki and H. S. Tharp, "Concurrent hyperthermia estimation schemes based on extended Kalman filtering and reduced-order modeling," *Int. J. Hyperthermia*, vol. 9, no. 6, pp. 849-865, 1993.

[20] E. A. Bailey, A. W. Dutton, M. Mattingly, S. Devasia, and R. B. Roemer, "A comparison of reduced-order modelling techniques for application in hyperthermia control and estimation," *Int. J. Hyperthermia*, vol. 14, no. 2, pp. 135-156, 1998.

[21] M. Mattingly, E. A. Bailey, A. W. Dutton, R. B. Roemer, and S. Devasia, "Reduced-order modeling for hyperthermia: An extended balanced-realization-based approach," *IEEE Trans. Biomed. Eng.*, vol. 45, no. 9, pp. 1154-1162, September 1998.

[22] M. Mattingly, *Modeling and control: Theoretical development with application to hyperthermia cancer therapy.* Ph.D. thesis, University of Utah, Appendix C, 1998.

[23] V. Druskin and L. Knizhnerman, "On application of the Lanczos method to solution of some partial differential equations," *J. Comp. Apppl. Math.*, vol. 50, pp. 255-262, 1994.

[24] V. Druskin and L. Knizhnerman, "The Lanczos optimization of a splitting-up method to solve homogeneous evolutionary equations," *J. Comp. Apppl. Math.*, vol. 42, no. 2, pp. 221-231, 1992.

[25] B. Nour-Omid, "Lanczos method for heat conduction analysis," *Inernat. J. Numer. Methods Engrg.*, vol. 24, no. 1, pp. 251-262, 1987.

[26] C. Gabriel, S. Gabriel, and E. Corthout, "The dielectric properties of biological tissues: I. Literature survey," *Phys. Med. Biol.*, vol. 41, pp. 2231-2249, 1996.

[27] S. Gabriel, R. W. Lau, and C. Gabriel, "The dielectric properties of biological tissues: III. Parametric models for the dielectric spectrum of tissues," *Phys. Med. Biol.*, vol. 41, pp. 2271-2293, 1996.

[28] K. S. Yee, "Numerical solution of initial boundary value problems involving Maxwell's equations in isotropic media," *IEEE Trans. Antennas Propagat.*, vol. 14, pp. 302–307, 1966.

[29] C.-Q. Wang and O. P. Gandhi, "Numerical simulation of annular phased arrays for anatomically based models using the FDTD method," *IEEE Trans. Microwave Theory Tech.*, vol. 37, no. 1, pp. 118–126, January 1989.

[30] D. M. Sullivan, "Three-dimensional computer simulation in deep regional hyperthermia using the finite-difference time-domain method," *IEEE Trans. Microwave Theory Tech.*, vol. 38, no. 2, February 1990.

[31] J.-Y. Chen and O. P. Gandhi, "Numerical simulation of annular-phased arrays of dipoles for hyperthermia of deep-seated tumors," *IEEE Trans. Biomed. Eng.*, vol. 39, no. 3, pp. 209–216, March 1992.

[32] K. D. Paulsen, S. Geimer, J. Tang, and W. E. Boyse, "Optimization of pelvic heating rate distributions with electromagnetic phased arrays," *Int. J. Hyperthermia*, vol. 15, no. 3, pp. 157-186, 1999.

[33] H. H. Pennes, "Analysis of tissue and arterial blood temperatures in the resting human arm," *J. Appl. Physiol.*, vol. 1, pp 93–122, 1948.

[34] E. Hutchinson, M. Dahleh, and K. Hynynen, "The feasibility of MRI feedback control for intracavity phased array hyperthermia treatments," *Int. J. Hyperthermia*, vol. 14, no. 1, pp. 39–56, 1998.

[35] P. Bernadi, M. Cavagnaro, S. Pisa, and E. Piuzzi, "SAR distribution and temperature increase in an anatomical model of the human eye exposed to the field radiated by the user antenna in a wireless LAN," *IEEE Trans. Microwave Theory Tech.*, vol. 46, no. 12, pp. 2074-2082, December 1998.

[36] G. H. Golub and C. F. Van Loan, *Matrix Computations, 3rd ed.* Baltimore, MA: Johns Hopkins University Press, 1996, Chapter 9.

[37] R. F. Remis and P. M. van den Berg, "Efficient computation of transient diffusive fields by a reduced modeling technique," *Radio Science*, vol. 33, no. 2, pp. 191-204, March-April 1998.

[38] E. Chiprout and M. S. Nakhla, *Asymptotic waveform evaluation and moment matching for interconnect analysis.* Boston, MA: Kluwer Academic Publishers, 1994.

[39] P. Dorato, C. Abdallah, and V. Cerone, *Linear-Quadratic Control: An Introduction.* Englewood Cliffs, NJ: Prentice Hall, 1995, Chapter 3.

[40] K. Ocheltree and L. Frizzell, "Determination of power deposition patterns for localized hyperthermia: A transient analysis," *Int. J. Hyperthermia*, vol. 4, no. 3, pp. 281-296, 1988.

[41] D. G. Luenberger, *Introduction to Linear and Nonlinear Programming.* Reading, MA: Addison-Wesley Publishing Company, 1973.

[42] P. VanBaren and E. S. Ebbini, "Multipoint temperature control during hyperthermia treatments: theory and simulation," *IEEE Trans. Biomed. Eng.*, vol. 42, no. 8, pp. 818–827, August 1995.

[43] F. Bardati, G. Gerosa, and P. Lampariello, "Temperature distribution in simulated living tissues irradiated electromagnetically," *Alta Frequenza*, vol. XLIX, no. 2, pp. 61-67, March-April 1980.

[44] J. Lang, B. Erdmann, and M. Seebass, "Impact of nonlinear heat transfer on temperature control in regional hyperthermia," *IEEE Trans. Biomed. Eng.*, vol. 46, no. 9, pp. 1129-1138, September 1999.

[45] I. G. Zubal, C. R. Harrell, E. O. Smith, Z. Rattner, G. Gindi, P. B. Hoffer, "Computerized three-dimensional segmented human anatomy," *Med. Phys.*, vol. 21, no. 2, pp. 299-302, 1994.

[46] F. A. Duck, *Physical Properties of Tissue: A Comprehensive Reference.* London: Academic Press, 1990.